Scientific Research Publishing

Open Journal of Applied Sciences, 2026, 16(1), 168-197
https://www.scirp.org/journal/ojapps
ISSN Online: 2165-3925
ISSN Print: 2165-3917

Facies-Specific NaOH-Activated Gold Tailings from Senegal for Non-Load-Bearing Masonry Units: Mix Design, Strength and Leaching Performance

Ibrahima Dia[1*], Souleymane Niang[1], Babacar Diouf[2]

[1]Polytech Diamniadio, Amadou Mahtar Mbow University, Dakar, Senegal
[2]Faculty of Engineering Sciences, Iba Der Thiam University, Thies, Senegal
Email: *ibrahima.dia@uam.edu.sn

How to cite this paper: Dia, I., Niang, S. and Diouf, B. (2026) Facies-Specific NaOH-Activated Gold Tailings from Senegal for Non-Load-Bearing Masonry Units: Mix Design, Strength and Leaching Performance. *Open Journal of Applied Sciences*, **16**, 168-197.
https://doi.org/10.4236/ojapps.2026.161011

Received: December 20, 2025
Accepted: January 10, 2026
Published: January 13, 2026

Abstract

The distinct oxidized and sulfidic facies of Sabodala gold mine tailings (Senegal), characterised by near-neutral drainage, are evaluated as potential secondary raw materials for non-load-bearing masonry in West Africa. This study evaluates NaOH-activated tailings as alkali-activated binders, examining mechanical performance, water absorption, leaching behavior, preliminary durability and curing energy demand. Both facies were activated with NaOH solutions of varying molarity and solution-to-solids ratio, with minor additions (~3 wt%) of Portland cement or hydrated lime and curing temperatures up to 210˚C. NaOH molarity emerged as the primary strength driver, while solution fraction defined facies-specific optima at ~21 wt% (oxidized) and ~18 wt% (sulfidic). Within this window, under 210˚C/4 h curing, 28-day compressive strengths reached 12 - 20 MPa with 24 h water absorption of 10% - 15%. Product leachates for As, Cd, Cr, Cu, Ni, Pb and Zn remained low and within indicative construction product limits. Accelerated wet-dry and sulfate exposure tests showed strength retention generally above ~80%, though these represent short-term screening rather than full service-life assessment. The consistent flexural-compressive strength relationship (ft ~ 0.26 - 0.27 fc) enables compression-based quality control. Overall, this work establishes practical, facies-specific mixture windows for NaOH-activated Sabodala tailings as secondary mineral resources, guiding the development of lower-energy curing schedules and supporting future standardization of tailings-based masonry units and mine-tailings management strategies.

Keywords

Gold-Mine Tailings, Alkali-Activated Materials, Masonry Units, Non-Load-Bearing Blocks, West Africa

1. Introduction

Mine tailings represent one of the largest industrial waste streams worldwide, posing significant environmental and socio-economic challenges. Beyond engineered storage, repurposing geochemically benign tailings as construction materials aligns with circular-economy and sustainable mine-closure strategies. In this perspective, carbonate-buffered gold tailings can be regarded as secondary mineral resources rather than waste, which is central to contemporary minerals engineering practice. In rapidly urbanising regions like West Africa, where demand for masonry units outpaces local availability of quality aggregates, converting suitable tailings into masonry products can support local supply chains while reducing environmental footprints [1]-[4].

Alkali-activated materials offer a proven pathway to valorise silicate-rich residues into binders with competitive strength and durability [5]-[11]. While extensive research has established the fundamental chemistry and microstructural development of these systems, recent work has expanded to include various industrial by-products, including mine tailings [12]-[14]. Studies report 28-day compressive strengths suitable for masonry applications and, in some cases, reduced leachability of potentially toxic elements [15] [16].

Gold-mine tailings constitute a specific subset within this field. Previous investigations demonstrate that gold-processing residues can develop substantial strength through alkali activation, with potential for trace metal immobilization [17]-[22]. However, most studies remain focused on paste or mortar-scale optimisation, with limited product-level assessment of strength, water absorption and leaching against masonry standards such as EN 771-1 and EN 771-3 or ASTM C62/C67 [23]-[26]. Practical guidance for converting specific gold tailings into compliant masonry products therefore remains scarce.

Geochemically, much tailings research addresses acid-generating systems, where low pH and sulphide oxidation drive metal release. In contrast, carbonate-buffered tailings with near-neutral drainage present lower metal mobility and greater reuse potential. The Sabodala gold operation in Senegal (**Figure 1**) exemplifies this favourable context, with distinct oxidized and sulfidic facies exhibiting near-neutral drainage. However, the fine-grained nature and low bearing capacity of these tailings necessitate stabilisation for construction applications [27]-[30].

Critical gaps persist for near-neutral gold tailings: facies-specific mix-design envelopes are undocumented; the combined effects of activation parameters on mechanical and hydric properties are rarely examined in an integrated way; and practical compressive-flexural strength relationships remain unquantified.

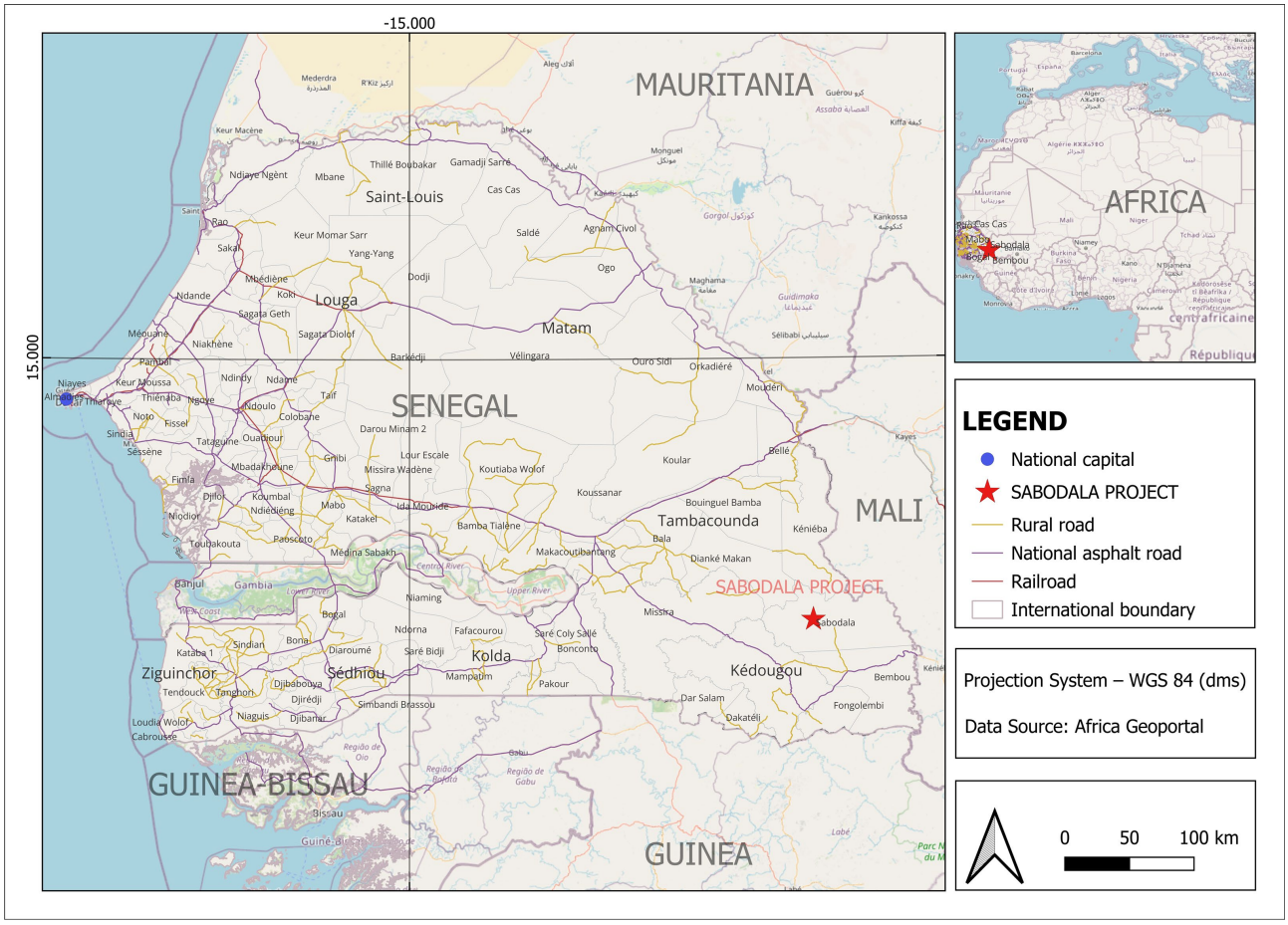

Figure 1. Location of the Sabodala gold mine in eastern Senegal, showing the main regional towns, infrastructure and national borders. Inset: position of Senegal within West Africa.

Previous work on alkali-activated mine tailings has mainly targeted copper, iron and polymetallic residues, typically in acid-generating systems, tested at paste scale and without explicit distinction between contrasting tailings facies. Consequently, there is currently no facies-specific mix-design framework for near-neutral, carbonate-buffered gold tailings in the West African Craton, and little information on how compressive and flexural strength, leaching behavior and short-term durability covary at product scale. This study addresses these gaps by investigating NaOH activation of oxidized and sulfidic facies from Sabodala tailings for non-load-bearing masonry. Specifically, we (i) delineate facies-specific activation windows based on NaOH molarity and activator solution fraction; (ii) quantify how activation parameters and curing regime jointly control compressive and flexural strength, density and 24 h water absorption; and (iii) assess product-level leaching and short-term durability against masonry benchmarks, thereby linking mix design to both mechanical and environmental performance. By integrating facies-specific optimisation with a comprehensive performance evaluation, we provide a practical framework for developing tailings-based masonry units in West African settings.

2. Materials and Methods

2.1. Materials

Process tailings from the Sabodala gold mine in eastern Senegal were used as the primary precursor. The ore is treated by conventional crushing and grinding, gravity and flotation, and the tailings are discharged into a downstream-raised tailings storage facility (TSF). Two representative facies were investigated: an oxidized facies sampled near the beach and an underlying sulfidic facies sampled closer to the pond. These facies were selected to capture the range of mineralogical and geochemical behavior relevant for potential reuse as construction materials. The main processing steps and the generation of oxidized and sulfidic tailings are summarized in Figure 2.

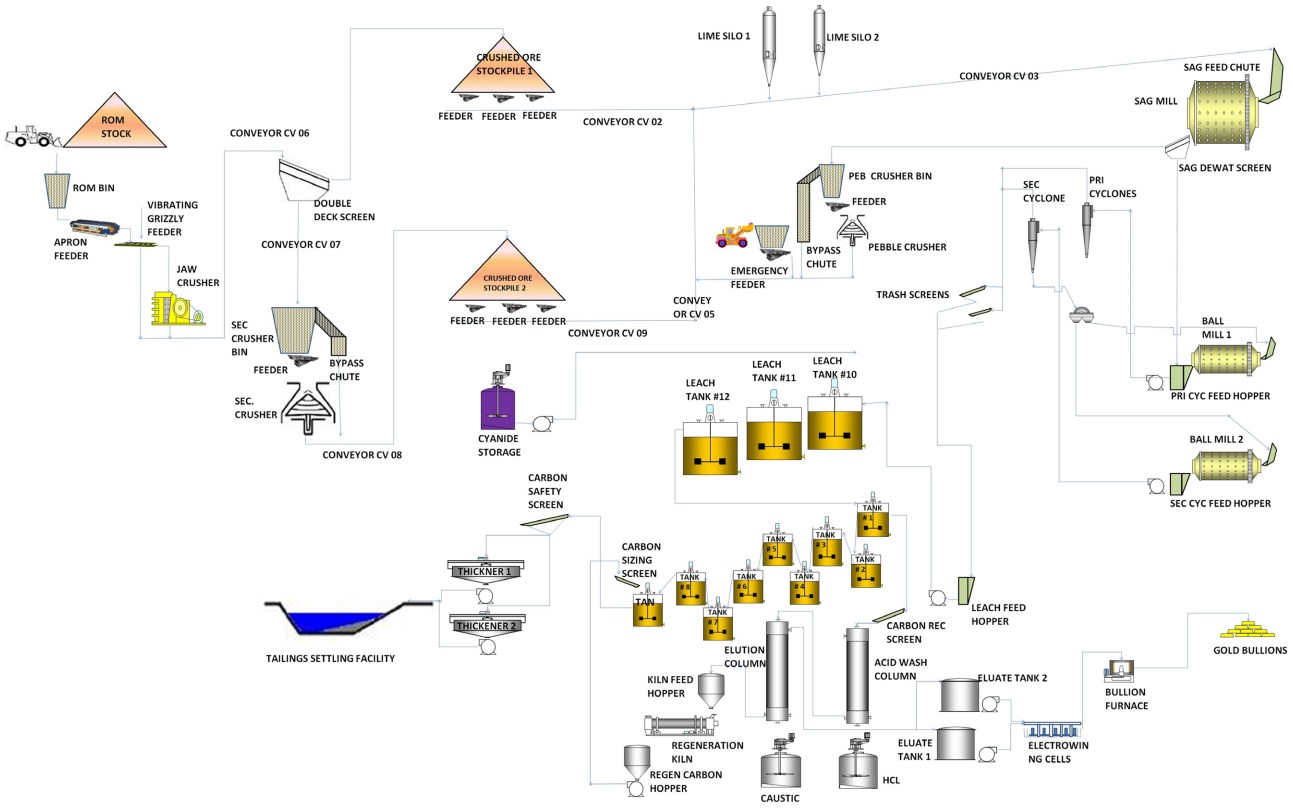

Figure 2. Simplified process flowsheet for ore processing and tailings generation at the Sabodala gold mine, highlighting the main steps leading to deposition of oxidized and sulfidic tailings in the TSF.

Tailings were sampled by combining near-surface channel samples, auger borings and shallow pits distributed across the TSF (Figure 3). Composite samples were air-dried, gently disaggregated and sieved to remove occasional gravel-size particles (>4 mm). Before mix preparation, moisture content was measured and all mix proportions were corrected to a dry-mass basis. Subsamples were stored in airtight containers prior to testing to minimize moisture exchange.

Bulk chemical composition of the oxidized and sulfidic tailings was determined by X-ray fluorescence (XRF) on dried, powdered subsamples. Major oxides are

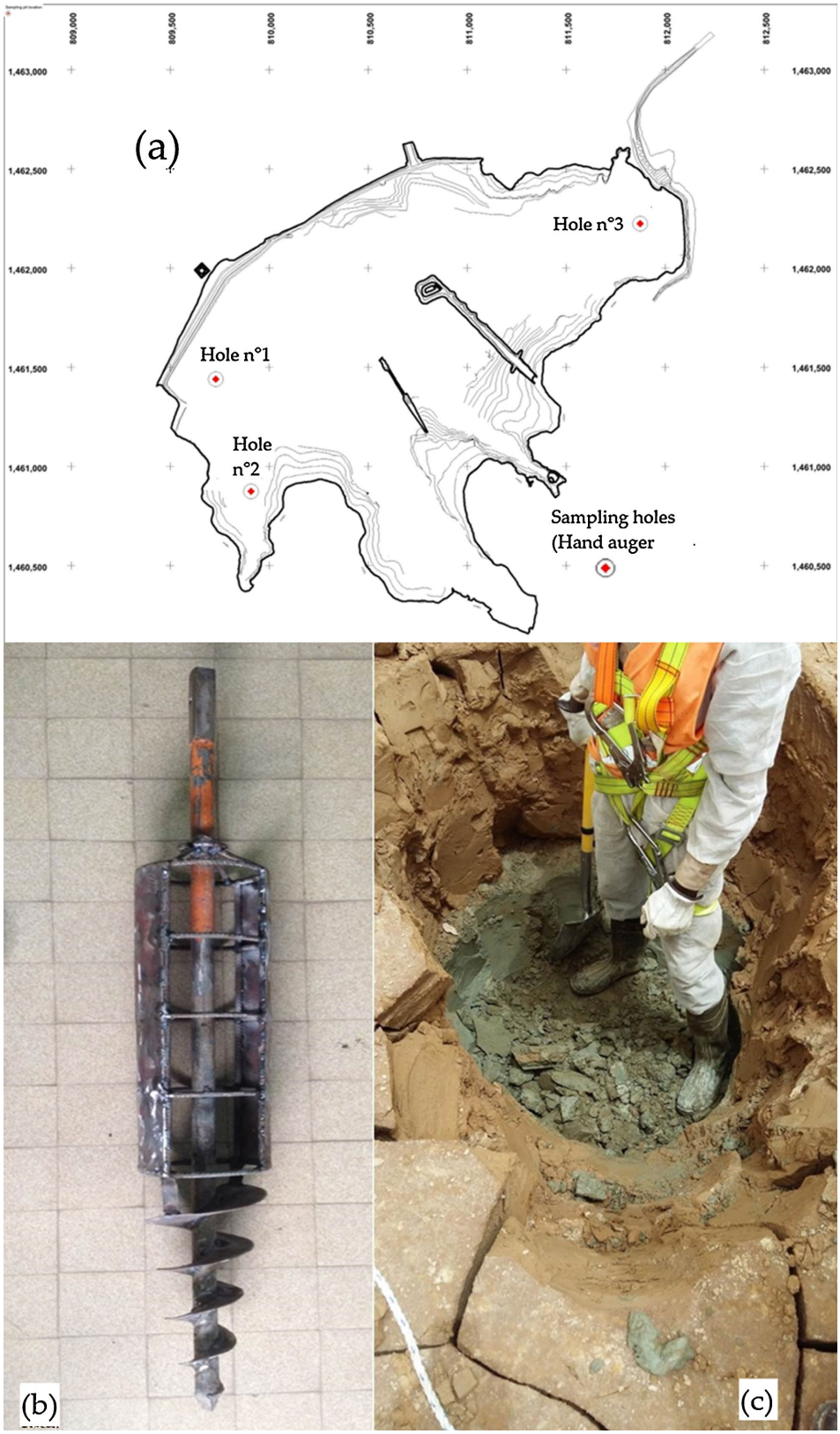

Figure 3. Sampling of oxidized and sulfidic tailings at the Sabodala TSF: (a) plan view of the tailings storage facility showing the locations of auger holes and hand-dug pits; (b) hand auger used for core recovery; (c) field sampling in a shallow pit intersecting the sulfidic facies.

reported as wt% together with loss on ignition (LOI) and total sulfur (S, or SO3-equivalent where applicable). These quantitative data are provided in the Results (Section 3.4.4) to substantiate the mineralogical and geochemical distinctions between facies.

Basic geotechnical characterization of the tailings included particle size distribution, Atterberg limits, methylene blue value, Proctor compaction and California Bearing Ratio (CBR) tests carried out using standard procedures. Field dry unit weights were also measured on both facies. Mineralogical and geochemical characterization relied on bulk powder X-ray diffraction (XRD) and whole-rock chemistry (XRF major oxides, LOI and total sulfur) to identify the main crystalline phases and to quantify the abundance of carbonates and sulfides. The corresponding results and their implications for geotechnical suitability and geochemical behavior are presented in Section 3.4.

The alkaline activator was an aqueous sodium hydroxide (NaOH) solution prepared from solid pellets (≥98% purity) dissolved in deionized water (conductivity ≤ 5 μS·cm^{-1}). Minor additions of Portland cement (CEM I 42.5 N) and hydrated lime were used as auxiliary binders to explore their influence on strength and water absorption. Unless otherwise stated, all dosages are expressed as mass fractions relative to the dry mass of tailings [31]. In contrast to many studies that rely on mixed NaOH-sodium silicate activators [5]-[11] [13] [15] [16], NaOH alone was used here. This choice reflects the ready availability and lower cost of caustic soda in the Senegalese mining context, as well as the high inherent silica and feldspar content of the tailings, which reduces the need for additional soluble silicate. Focusing on NaOH also simplifies potential field implementation and process control.

2.2. Mix Design Variables

The mix design focused on four main variables:

- NaOH molarity, varied between 5 and 8 mol·L^{-1};
- Activator solution fraction, defined as the mass of NaOH solution per mass of dry tailings, typically in the range 16-22 wt%;
- Auxiliary binder content, with cement or lime additions between 0 and 6 wt% of dry tailings;
- Curing temperature and age, with thermal curing temperatures between 110 and 300˚C (representative condition 210˚C for 4 h) and testing at 7 and 28 days.

Oxidized and sulfidic tailings were treated as separate precursors so that facies-dependent optima in activator content and curing conditions could be identified. A screening phase combined one-factor-at-a-time (OFAT) series with a reduced second-order response-surface design of Box-Behnken type. In this design, each facies was explored with a limited number of mixes, using three levels for each factor spanning the practically relevant ranges: NaOH molarity across 5 - 8 M, activator solution fraction across 16 - 22 wt%, auxiliary binder content across 0 - 6 wt% and curing temperature across 150˚C - 250˚C (with 210˚C/4 h as the central

condition). These ranges were selected to target compressive strengths and water absorption compatible with non-load-bearing masonry classes in common standards (EN/ASTM/AFNOR), as further discussed in the Results and Discussion.

2.3. Specimen Preparation and Curing

Unless otherwise indicated, mass fractions of activator solution and auxiliary binders are given relative to the dry mass of tailings. For each mix, the required amount of NaOH solution was prepared at least 24 h in advance to allow cooling to laboratory temperature and stabilization of molarity.

Dry tailings and the selected cement or lime addition were premixed for approximately 2 min in a paddle mixer. The pre-measured NaOH solution was then added over ~30 s while mixing continued for a further 3 - 4 min to obtain a homogeneous paste. The fresh mix was cast into prismatic molds (nominal dimensions 40 × 40 × 160 mm) in two layers, each compacted by light vibration and rodding to remove entrapped air. Molds were sealed to limit moisture loss and stored at (20 ± 2)˚C for 24 h.

After demolding, two curing regimes were applied:

- Sheltered drying at ambient conditions, where specimens were stored under shelter at (20 ± 2) ˚C and ~50% - 60% relative humidity for up to 28 days;
- Thermal curing, where specimens were first dried at (40 - 50)˚C to constant mass, then placed in a ventilated oven at the target curing temperature between 110 and 300˚C. Unless otherwise stated, a representative curing schedule of 210˚C for 4 h was used.

The high-temperature curing regime was selected as an upper-bound, exploratory condition to clearly delimit a robust formulation window; subsequent work will aim at reducing curing temperatures and times. Such a curing schedule is much lower in temperature and duration than typical firing of clay bricks (often 800˚C - 1000˚C for many hours), but still significantly more energy-intensive than the ambient or low-temperature curing regimes used for Portland cement-based masonry units.

Preliminary trials indicated that thermal curing is required to achieve significant strength development in these tailings; quantitative strength results for the different curing regimes are presented in Section 3.1. After thermal curing, specimens were allowed to cool to room temperature before subsequent conditioning and testing.

A first-order estimate of the specific energy consumption associated with oven curing (kWh·kg^{-1} of product) was derived from logged oven power, duty cycle and batch mass.

2.4. Mechanical and Physical Testing

For each formulation × curing condition, approximately 10 - 12 prisms were cast, providing at least 6 replicate specimens per test age for mechanical measurements. Flexural-tensile and compressive strength tests followed EN 196-1 procedures

adapted to alkali-activated units. Flexural-tensile strength was measured in three-point bending on 40 × 40 × 160 mm prisms; the two halves generated by flexural failure were then used for compressive strength testing. Strengths are reported as peak load divided by the loaded area and expressed in MPa. Loading rates were selected to be consistent with EN 196-1 recommendations (of the order of 0.05-0.10 $kN \cdot s^{-1}$ for flexure and 2.4 ± 0.2 $kN \cdot s^{-1}$ for compression). Unless otherwise stated, mean strength and absorption values reported in Section 3 (Results) are based on n = 6-8 specimens per mix and test age.

Water absorption and bulk dry density were determined on specimens subjected to the prescribed curing schedule. After curing, specimens were dried at (40 - 50)˚C to constant mass, cooled in a desiccator and weighed to obtain the dry mass. For water absorption tests, dried specimens were immersed in water at (23 ± 2)˚C and weighed after 24 h and after 6 days of immersion. Water absorption was calculated as the percentage increase in mass relative to the dry mass. Bulk dry density was calculated from the dry mass and the post-cure specimen volume; the latter was determined from three orthogonal dimensions (length, width, height) measured with a digital calliper (±0.1 mm). Specimens with obvious edge damage or chipped corners were discarded and replaced to avoid volume bias.

2.5. Durability Testing

Two accelerated durability protocols were implemented on representative mixes selected to span the main formulation variables (facies, NaOH molarity, solution fraction near the identified optimum, and type of auxiliary binder):

- Wet-dry cycling: each cycle consisted of 24 h water immersion at (23 ± 2)˚C followed by 24 h oven drying at (50 ± 2)˚C. Specimens were subjected to up to 25 cycles. Flexural and compressive strengths were measured after 0, 10 and 25 cycles to assess strength retention and visible damage (cracking, scaling, spalling).
- Sulfate exposure: specimens were immersed in sodium sulfate (Na_2SO_4, 50 $g \cdot L^{-1}$) and magnesium sulfate ($MgSO_4$, 50 $g \cdot L^{-1}$) solutions at (23 ± 2)˚C. The Na_2SO_4 concentration (≈5% by mass, ~50 $g \cdot L^{-1}$) follows the commonly used sulfate solution specified in ASTM C1012/C1012M [32] for sulfate resistance testing. A liquid-to-solid ratio of 10 $L \cdot kg^{-1}$ was used, and solutions were renewed every 7 days to maintain sulfate concentration. Mass change, surface condition and the penetration depth of reaction fronts (assessed with phenolphthalein indicator on fractured surfaces) were monitored after 28 days of exposure.

These two protocols were selected as simple representations of intermittent wetting-drying and sulfate-rich exposure conditions that are relevant for masonry units in many Sahelian and Sudanian settings, where walls may experience episodic rainfall and contact with sulfate-bearing soils or groundwater.

For each durability condition, three to four specimens were tested. All mechanical tests were performed on a calibrated electromechanical testing frame with appropriate load cell and crosshead speed settings for mortar-sized specimens.

These durability protocols were conceived as short-term screening tests rather than full durability qualification.

2.6. Product-Level Leaching

Leaching of the cured products was evaluated on mechanically tested prisms using the EN 12457-2 batch leaching test. Fragments were crushed to <4 mm, and a liquid-to-solid ratio of 10 $L \cdot kg^{-1}$ deionised water was applied [33]. The suspensions were agitated for 24 h at (20 ± 2)˚C and then filtered. The final pH of each filtrate was measured immediately after filtration using a calibrated pH meter and is reported alongside the metal concentrations (see Section 3.5). Filtrates were analysed for major and trace elements of interest, including As, Cd, Cr, Cu, Ni, Pb and Zn, by inductively coupled plasma optical emission spectrometry (ICP-OES). Analytical quality was checked using procedural blanks, duplicate samples and certified reference materials. Typical limits of detection for the monitored trace metals were on the order of 1 - 20 $\mu g \cdot L^{-1}$, depending on the element. For the purpose of summary statistics, concentrations reported as below the detection limit were assigned a value of one half of the corresponding detection limit.

To provide environmental context for potential reuse, leachate concentrations were compared with indicative limit values compiled from European guidance documents on leaching from construction products and recycled materials, such as CEN technical specifications on the release of dangerous substances and Council Decision 2003/33/EC. These comparisons are used only as non-regulatory benchmarks; formal compliance assessments would require testing on full-size units under the specific regulatory framework of the country of use. The detailed comparison with limit values is presented in the Results (Section 3.5). Statistical differences in leachate composition between mix types were assessed at a significance level $\alpha = 0.05$.

2.7. Microstructural Characterisation

Mercury intrusion porosimetry (MIP) was used to quantify total porosity and pore size distribution in selected mixes representative of key formulation windows. Fragments of cured prisms (~5 - 10 mm) were taken after mechanical testing, oven-dried at (40 - 50)˚C to constant mass and analysed in an automated porosimeter. The applied pressure range corresponded to an equivalent pore-throat radius range of approximately 0.005 - 100 μm. Duplicate runs and periodic drift checks with manufacturer standards were performed to ensure data quality [34] [35]. Cumulative intrusion curves and derived parameters (total porosity, modal pore radius and sub-0.1 μm pore fraction) are referenced in the Results.

Scanning electron microscopy (SEM) was carried out on carbon-coated fragments (~5 - 10 mm) of cured specimens taken after mechanical testing. Observations were made in backscattered electron mode at an acceleration voltage of 15 - 20 kV to enhance phase contrast. The focus was on the microstructure of the binder phase, reaction rims around unreacted tailings grains and crack patterns.

Powder X-ray diffraction (XRD) was used primarily to identify primary and secondary crystalline phases in the tailings and in selected cured products. Patterns were collected over a 2θ range of about 5˚ - 70˚ with a step size appropriate for phase identification, with emphasis on phases controlling alkali uptake and buffering, and to relate these features to the carbonate-buffered geochemical behavior established independently.

Fourier-transform infrared spectroscopy (FTIR) was also performed on selected powdered samples (raw tailings and cured products) to provide complementary information on the main functional groups present in the reaction products and on the evolution of aluminosilicate and carbonate bands during activation. Spectra were collected over the mid-infrared range with a standard resolution suitable for phase identification and band-shape analysis.

2.8. Experimental Design and Statistical Analysis

An OFAT-anchored experimental design was adopted to screen the main effects of NaOH molarity, activator solution fraction, auxiliary binder content, curing temperature and age, and facies. This screening was complemented by a reduced second-order response-surface design (Box-Behnken type) in the most relevant parameter ranges (NaOH 5 - 8 M; solution fraction 16 - 22 wt%; cement or lime 0 - 6 wt%; curing temperatures 150˚C - 250˚C, typically 210˚C/4 h; ages 7 and 28 days). This design enabled attribution of performance trends to individual variables and their interactions while limiting the total number of mixes per facies. For illustration, one oxidized-facies mix in the Box-Behnken matrix combined a 6 M NaOH solution at 19 wt% of the tailings with 4 wt% Portland cement and curing at 210˚C for 4 h, whereas a representative sulfidic-facies mix used 7 M NaOH at 20 wt%, 4 wt% hydrated lime and the same thermal curing schedule.

For selected response variables (primarily compressive and flexural-tensile strengths), second-order polynomial models were fitted as functions of the main design variables. Analysis of variance (ANOVA) was used to assess the significance of individual coefficients and overall model fit at $\alpha = 0.05$. Model assumptions (normality and homoscedasticity of residuals) were checked graphically and found acceptable for the retained models. Root-mean-square errors are expressed in MPa for strength responses and in percentage points for water absorption. All statistical analyses were performed in R (R Core Team, Vienna, Austria) using standard linear modelling functions. For the retained models, adjusted goodness-of-fit metrics and global F-tests indicate satisfactory fits for compressive strength, flexural-tensile strength and 24 h water absorption over the explored design space.

3. Results

3.1. Strength Development as a Function of Mix Design and Curing

Strength development in NaOH-activated Sabodala tailings is governed by the combined effects of activator concentration, activator solution fraction, auxiliary binder type and curing regime. Unless otherwise stated, reported values in this

section refer to 28-day strengths of thermally cured specimens.

Representative mean compressive strengths (fc), flexural-tensile strengths (ft), bulk dry densities and water absorption values for selected mixes are summarised in Table 1 for both oxidized and sulfidic facies. For each mix, Table 1 lists NaOH molarity, activator solution fraction, auxiliary binder type and content, curing temperature, number of specimens tested (n), and mean values with standard deviations.

Table 1. Representative 28-day mechanical properties, dry density and 24 h water absorption for selected NaOH-activated Sabodala tailings mixes within the validated process window.

Mix ID	Facies	NaOH molarity (M)	NaOH solution (wt% of tailings)	Auxiliary binder (type; wt%)	Curing (˚C; h)	n (specimens)	fc,28 (MPa, mean ± SD)	ft,28 (MPa, mean ± SD)	Dry density (kN·m^{-3}, mean ± SD)	WA24h (% mass, mean ± SD)
O-C3	Oxidized	8	21	Portland cement; 3	210; 4	7	14.5 ± 1.2	3.9 ± 0.4	17.8 ± 0.3	13.5 ± 0.6
O-L3	Oxidized	8	21	Hydrated lime; 3	210; 4	7	16.5 ± 1.3	4.4 ± 0.5	17.5 ± 0.3	14.8 ± 0.7
S-C3	Sulfidic	8	18	Portland cement; 3	210; 4	8	19.0 ± 1.5	5.0 ± 0.5	18.6 ± 0.4	10.8 ± 0.5
S-L3	Sulfidic	8	18	Hydrated lime; 3	210; 4	8	17.0 ± 1.4	4.4 ± 0.5	18.1 ± 0.4	12.2 ± 0.6

3.1.1. Effect of NaOH Molarity

Increasing NaOH concentration from 5 to 8 M consistently increased both fc and ft for both facies at fixed activator solution fraction, auxiliary binder content and curing schedule. For mixes without auxiliary binder, raising NaOH from 5 to 8 M moved 28-day fc from the lower part of the 10 - 15 MPa range to values approaching or exceeding 15 - 18 MPa in optimised compositions (Table 1). This trend was further amplified in the presence of cement or lime.

Response-surface analysis confirmed that NaOH molarity is a first-order driver of strength, with a statistically significant positive main effect ($p < 0.05$) over the explored 5 - 8 M range. These effects are illustrated for representative mixes in Figure 4(a), together with the influence of Portland cement content in Figure 4(b).

3.1.2. Effect of Activator Solution Fraction

For a given NaOH molarity and auxiliary binder system, the activator solution fraction (mass of NaOH solution per mass of dry tailings) exerted a strong, nonlinear control on strength. Strength increased with solution fraction up to facies-dependent optima near ~21 wt% for oxidized tailings and ~18 wt% for sulfidic tailings, then decreased at higher solution contents. Below these optima, incomplete wetting and limited gel formation led to lower strengths and higher scatter. Above them, excess solution was associated with higher capillary porosity and enhanced drying shrinkage, resulting in reduced fc and ft. These trends are captured

by the quadratic terms in the response-surface models and are illustrated in the two-dimensional projections shown in Figure 5.

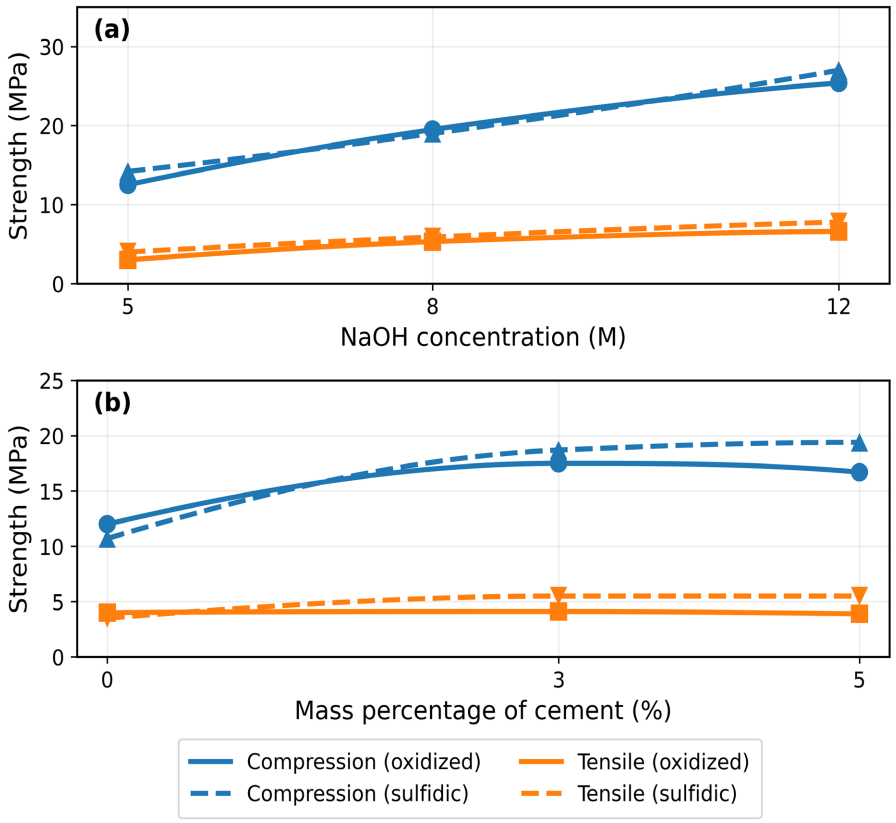

Figure 4. Effect of (a) NaOH concentration and (b) Portland cement dosage on 28-day compressive and flexural-tensile strengths of NaOH-activated Sabodala tailings for oxidized and sulfidic facies.

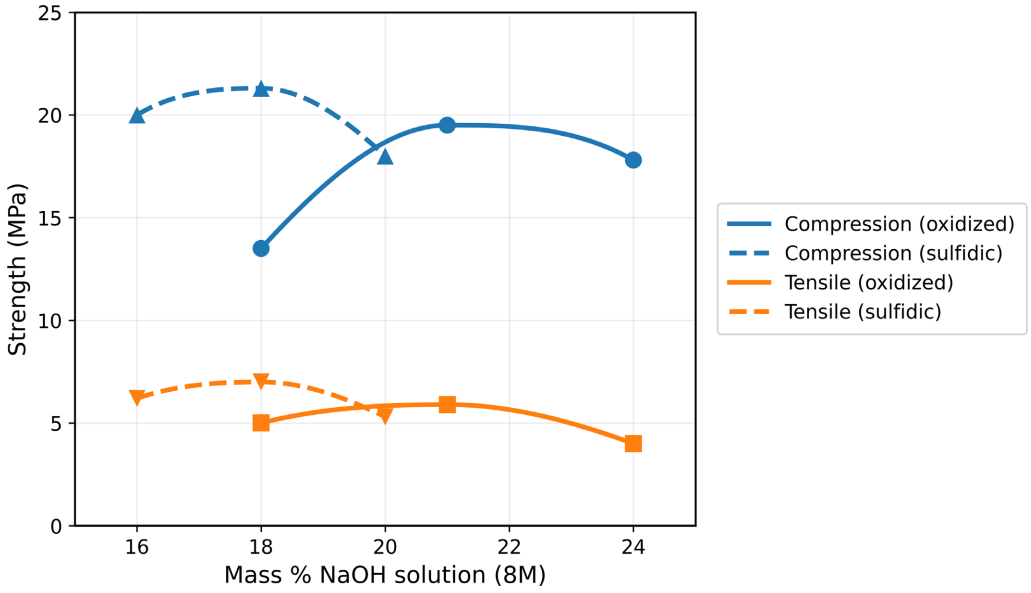

Figure 5. Effect of activator solution mass fraction (8 M NaOH) on 28-day compressive and flexural-tensile strengths of NaOH-activated Sabodala tailings for oxidized and sulfidic facies.

3.1.3. Effect of Auxiliary Binder Content and Type

At fixed NaOH molarity (typically 8 M), solution fraction near the facies-specific optimum and curing at 210˚C for 4 h, the addition of small amounts of Portland cement or hydrated lime improved mechanical performance (Table 1). Increasing cement content up to about 3 - 4 wt% consistently raised fc and ft, with diminishing returns or slight decreases at higher dosages. Lime additions had a similarly positive effect, especially for the oxidized facies, where some formulations reached the upper part of the 12 - 20 MPa range. Under identical NaOH and solution conditions, lime-bearing mixes in oxidized tailings often achieved slightly higher fc than cement-bearing mixes, at the cost of somewhat higher water absorption (Section 3.3). These trends are consistent with the formation of additional calcium-rich hydrates that complement the alkali-activated gel in a carbonate-buffered system. Representative 7-day responses as a function of auxiliary binder content are shown in Figure 6.

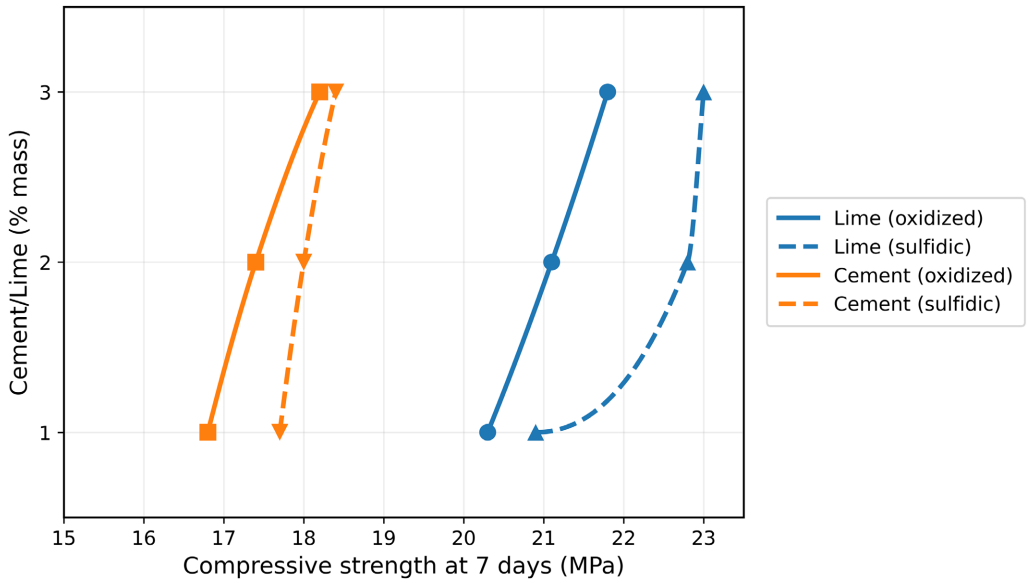

Figure 6. Influence of auxiliary binder type and dosage (Portland cement vs hydrated lime) on 7-day compressive strength of NaOH-activated Sabodala tailings for oxidized and sulfidic facies. Each curve links mixes with increasing auxiliary binder content (mass% of tailings).

3.1.4. Effect of Curing Temperature and Schedule

Thermal curing had a pronounced effect on strength. For both facies, 28-day fc increased when curing temperature was raised from 110˚C to around 210˚C, with little or no further gain at higher temperatures for most mix combinations. A sulfidic series at 8 M NaOH tolerated curing up to 300˚C with continued strength increases, but the majority of mixes showed plateaus or modest declines beyond 210˚C - 240˚C, suggesting a practical upper bound around 210˚C for routine curing. Without thermal curing, 28-day fc remained below 2 MPa, confirming that oven curing is essential for these tailings. A curing schedule of 210˚C for 4 h was therefore adopted as the reference condition for most comparative series and for the mixes summarised in Table 1. The dependence of compressive and flexural-

tensile strengths on curing temperature is illustrated in Figure 7 for both facies and NaOH molarities.

The need for elevated curing temperatures is consistent with the mineralogical nature of the Sabodala tailings. The raw materials are dominated by quartz and feldspar with significant carbonates and subordinate sulfides (Section 3.4.3), *i.e.*, a largely crystalline framework with limited highly reactive amorphous aluminosilicate phases. In such quartz-feldspar-carbonate systems, dissolution kinetics at low temperature are slow, while carbonates buffer the pore solution and consume part of the added OH−, reducing the effective activator availability for alkali-activated gel formation. Thermal curing therefore accelerates dissolution and promotes faster precipitation/condensation of binding gels (N-A-S-H and/or Ca-bearing gels), while also driving water removal and pore refinement. These constraints are more pronounced than in typical fly ash or slag systems, explaining why a ~210˚C schedule was required here to obtain product-level strengths within practical timeframes.

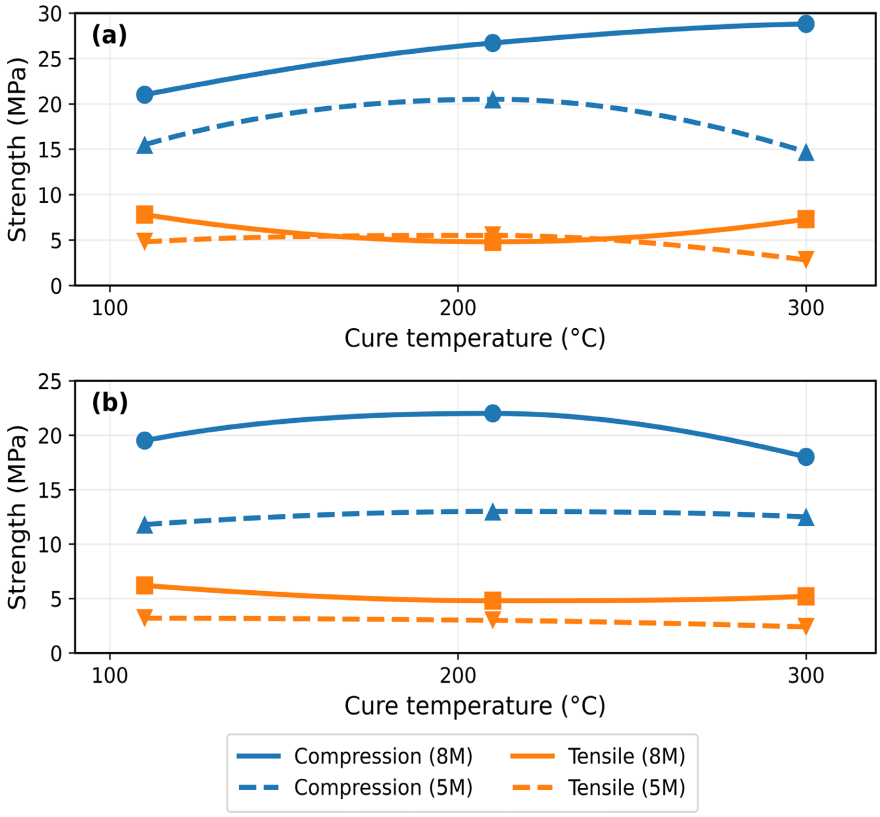

Figure 7. Effect of curing temperature on 28-day compressive and flexural-tensile strengths of NaOH-activated Sabodala tailings: (a) sulfidic facies and (b) oxidized facies, for mixes activated with 5 M and 8 M NaOH.

3.1.5. Effect of Age and Drying Regime

Strength generally increased from 7 to 28 days for thermally cured specimens, reflecting continued reaction and structural rearrangement. Early-age strengths measured on specimens stored under sheltered conditions (20˚C ± 2˚C, ~50% -

60% RH) were typically lower and more variable than those of oven-dried specimens, whereas by 28 days these differences largely diminished. These observations indicate that drying history primarily affects early-age response, while longer-term strengths depend mainly on mix design and thermal curing.

Within the validated process window (NaOH 5 - 8 M, facies-specific solution fractions near 18 - 21 wt%, auxiliary binder ~3 wt% and curing at ~210˚C/4 h), representative 28-day fc values for the best-performing mixes lie in the 12 - 20 MPa range (Table 1). These strength values were obtained on 40 × 40 × 160 mm prisms, and their comparison with declared compressive strengths for full-size masonry units in EN 771-3 and ASTM C55 [23]-[26] [36] should therefore be regarded as indicative only. For comparison, national implementations of EN 771-3 for aggregate concrete masonry units often declare mean compressive strengths on the order of 5 - 7.5 MPa for standard-density blocks used in non-load-bearing walls, depending on group and national annex, while ASTM C55 specifies minimum average compressive strengths of around 17 MPa for normal-weight concrete building brick together with maximum water absorption limits depending on weight classification. The 12 - 20 MPa range obtained here thus overlaps or exceeds the lower end of compressive strength requirements for non-load-bearing applications, while remaining well below values typical of structural units. An indicative comparison of the obtained strengths and water absorption values with selected non-load-bearing masonry classes from these standards is provided in Table 2.

Table 2. Indicative comparison between representative Sabodala mixes and selected non-load-bearing masonry classes in EN 771-3 and ASTM C55 (non-regulatory benchmark).

Product class/guideline	Standard	Declared mean fc (MPa)/WA limit (%)	Representative Sabodala mix (from Table 1)	fc, 28 (MPa)	WA 24 h (%)	Indicative comment
Aggregate concrete masonry units, non-load-bearing (typical national implementations)	EN 771-3	fc ~ 5 - 7.5; WA often ≤ 16 - 20	O-C3 (oxidized + 3% cement)	14.5	13.5	fc well above minimum; WA within typical ranges; laboratory prisms only
Normal-weight concrete building brick, non-load-bearing	ASTM C55	fc ≥ 17 (~2500 psi); WA limits weight-class dependent	S-C3 (sulfidic + 3% cement)	19	10.8	fc close to or slightly above minimum; WA favourable; indicative only
Lightweight/hollow non-structural units (various national classes)	EN 771-3/ASTM C55	fc ~ 7.5 - 12; WA variable	O-L3 or S-L3 (3% lime)	16.5 - 17.0	12.2 - 14.8	Strength exceeds many non-load-bearing thresholds; WA moderate

3.2. Tensile-Compressive Strength Relationship

Flexural-tensile strength (ft) and compressive strength (fc) exhibit a strong, approximately linear relationship across the tested mixes and curing conditions. Linear regressions performed separately for each facies, pooling 7 and 28-day data,

yield proportionality factors of (Figure 8): Sulfidic facies: ft ~ 0.26 fc and Oxidized facies: ft ~ 0.27 fc.

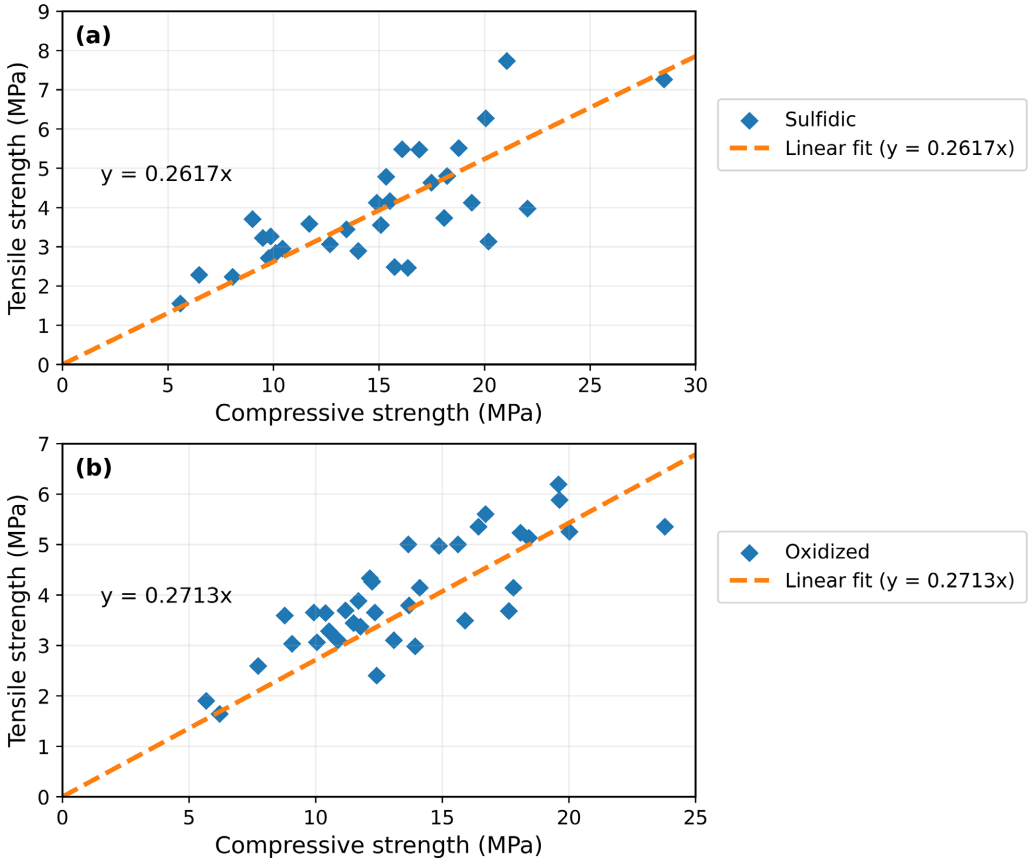

Figure 8. Relationship between flexural-tensile strength (ft) and compressive strength (fc) for NaOH-activated Sabodala tailings: (a) sulfidic facies and (b) oxidized facies. Symbols show individual 7- and 28-day prism test results; dashed lines are least-squares linear regressions (ft ~ 0.26 fc for sulfidic mixes and ft ~ 0.27 fc for oxidized mixes), with Pearson correlation coefficients r on the order of 0.75 - 0.77.

For the fc range covered by the experiments (approximately 8 - 22 MPa), most individual ft values fall within about ±15% - 20% of the corresponding regression line.

These relationships are not proposed as formal design equations in a normative sense, but as practical scaling laws. Within this formulation window, they support the use of compressive strength as a primary control parameter for mix optimisation and quality control, with flexural performance inferred from fc using conservative margins. The Discussion (Section 4.2) illustrates how these scaling laws can be used to define indicative ft ranges compatible with non-load-bearing masonry requirements based on compressive tests alone.

3.3. Density and Water Absorption

3.3.1. Bulk Dry Density

Bulk dry density showed limited sensitivity to mix design variables compared with strength. Across more than 300 stabilised prisms, mean dry densities of the cured

products remained below those of the untreated tailings, typically around 17 - 19 $kN \cdot m^{-3}$ depending on facies, compared with ~21 $kN \cdot m^{-3}$ for the raw materials. Mean values and standard deviations for representative mixes are reported in Table 1.

No systematic trends in density with NaOH molarity, solution fraction or auxiliary binder were observed within the tested ranges, indicating that these parameters primarily affect microstructural connectivity and pore structure rather than bulk compaction state. Plots of fc and 24 h water absorption versus dry density show no strong correlation between density and either mechanical strength or absorption, confirming that bulk density is a poor predictor of performance compared with capillary porosity and pore-size distribution.

3.3.2. Water Absorption

Water absorption tests on a subset of approximately 120 prisms showed systematic differences between additive systems and immersion duration. Table 3 summarises, for representative formulations, mean and standard deviation values of 24 h and 6-day water absorption, together with the number of specimens (n) for each case.

Table 3. 24 h and 6-day water absorption for representative NaOH-activated Sabodala mixes within the validated process window.

Mix ID	Facies	Auxiliary binder	n (specimens)	WA24h (% mass, mean ± SD)	WA6d (% mass, mean ± SD)
O-C3	Oxidized	3 wt% cement	6	13.5 ± 0.6	14.7 ± 0.6
O-L3	Oxidized	3 wt% lime	6	14.8 ± 0.7	15.5 ± 0.7
S-C3	Sulfidic	3 wt% cement	6	10.8 ± 0.5	11.6 ± 0.5
S-L3	Sulfidic	3 wt% lime	6	12.2 ± 0.6	13.0 ± 0.6

For mixes within the identified process window, 24 h water absorption values generally fall in the range of about 10% - 15%, with 6-day values of similar magnitude but consistently slightly higher than the 24 h values, reflecting continued water uptake with immersion duration. Cement-bearing mixes consistently exhibited the lowest 24 h and 6-day absorption values, followed by mixed cement+lime systems and lime-only systems. For optimised oxidized-tailings mixes, 24 h absorption values tend to lie towards the upper part of this range, whereas optimised sulfidic mixes show slightly lower 24 h absorption with comparable (but slightly higher) 6-day values.

In EN 771-3 [23] [24], typical maximum water absorption values for aggregate concrete masonry units depend on density class and exposure conditions, but non-load-bearing units with normal or medium density often allow moderate absorptions of this order, provided that wall detailing and surface protection are appropriate. In ASTM C55, maximum water absorption is also limited as a function of weight classification (for example, around 13 - 15 $lb \cdot ft^{-3}$ for many normal and

medium-weight concrete bricks). In this context, the absorption ranges obtained here are compatible with non-load-bearing masonry applications under moderate exposure conditions, recognising that exact acceptance will depend on the specific standard, unit geometry and national annex. In practice, units with 24 h absorptions of this order would generally be used with external renders or claddings on rain-exposed faces, and their performance in persistently saturated or freeze-thaw environments would require additional verification.

These trends support the use of 24 h water absorption as a practical proxy for capillary porosity, to be monitored alongside fc during mix optimisation and quality control.

3.4. Porosity and Microstructure

3.4.1. Microstructure of Alkali-Activated Products

Mercury intrusion porosimetry (MIP) on representative mixes confirmed that activator content, auxiliary binder type and curing temperature primarily affect pore structure rather than total porosity. Table 4 reports total porosity, modal pore-throat radius and the fraction of pores with equivalent radii below 0.1 μm for selected mixes spanning the formulation window.

Table 4. Mercury intrusion porosimetry (MIP) descriptors for selected mixes, highlighting differences between optimized and under-reacted microstructures.

Mix (representative)	Total intruded porosity (%)	Cumulative intrusion (mL·g^{-1})	Threshold diameter (μm)	Modal pore size (μm)	Pores < 0.1 μm (% of total porosity)
Sulfidic + cement (optimum L/S; 8 M; 210˚C/4 h)	18.6 ± 0.5	0.41 ± 0.01	0.22 ± 0.02	0.09 ± 0.01	54.3 ± 2.1
Oxidized + cement (optimum L/S; 8 M; 210˚C/4 h)	21.2 ± 0.6	0.47 ± 0.02	0.28 ± 0.03	0.14 ± 0.02	42.7 ± 1.9
Oxidized + lime (low solution fraction; 5 - 6 M; 150˚C/4 h)	24.8 ± 0.7	0.55 ± 0.02	0.36 ± 0.03	0.20 ± 0.03	31.5 ± 2.4

Optimised mixes displayed a clear shift of the pore-size distribution towards smaller pore-throat radii and higher fractions of fine pores compared with less reactive or under-cured mixes. Total porosity varied only moderately between mixes, but differences in modal pore radius and the proportion of sub-0.1 μm pores were consistent with strength and absorption trends: mixes with higher fc and lower water absorption exhibited more refined pore networks [37].

3.4.2. Geotechnical Behavior and Implications for Raw Tailings

Basic geotechnical test results for the raw tailings indicate fine-grained materials with median particle sizes in the silt range and medium plasticity indices, consistent with low to moderate plasticity behavior in Atterberg-based classifications. Standard Proctor tests yield maximum dry densities around 1.83 g·cm^{-3} (~18 kN·m^{-3}) at optimum water contents near 13.5%, and the associated CBR indices at this optimum are very low, confirming poor bearing capacity. Field measure-

ments give apparent dry unit weights of about 19.9 kN·m^{-3} for the oxidized facies and 21.3 kN·m^{-3} for the sulfidic facies, broadly consistent with the laboratory compaction data. Methylene blue values are compatible with low to moderate clay activity.

3.4.3. Mineralogy (XRD)

Bulk powder XRD patterns for representative tailings samples confirm that both oxidized and sulfidic facies are dominated by quartz and feldspar, with significant carbonate peaks and subordinate sulfides, consistent with a carbonate-buffered, near-neutral geochemical behavior (**Figure 9**). Taken together with the geotechnical results in Section 3.4.2, these properties indicate low suitability of the raw tailings as compacted granular fill and motivate their consideration as precursors for stabilised or alkali-activated masonry units rather than bulk fill.

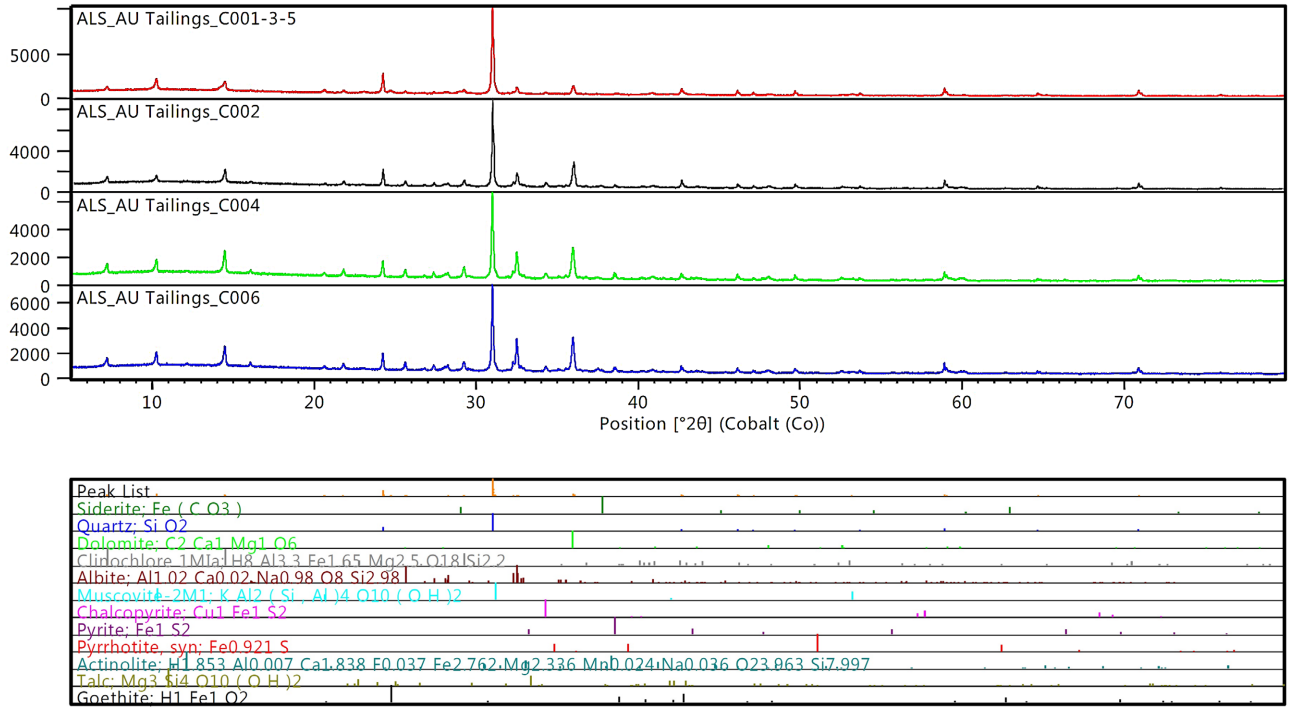

Figure 9. Powder X-ray diffraction (XRD) patterns for representative Sabodala tailings samples, showing quartz and feldspar-dominated mineralogy with abundant carbonates (e.g., siderite, dolomite, calcite) and subordinate sulfides (pyrite, pyrrhotite), consistent with carbonate-buffered, near-neutral geochemical behavior.

3.4.4. Bulk Chemical Composition (XRF)

XRF data indicate that both oxidized and sulfidic tailings are silica-rich, consistent with quartz-feldspar dominance (Section 3.4.3). The oxidized facies contain about 60.8 wt% SiO_2 and 11.2 wt% Al_2O_3, with moderate Fe_2O_3(t) (~5.5 wt%) and carbonate-related oxides CaO + MgO totaling ~9.5 wt% (CaO ~6.6 wt%, MgO ~2.9 wt%). In contrast, the sulfidic facies show slightly lower SiO_2 (~58.2 wt%) and Al_2O_3 (~10.6 wt%), but higher Fe_2O_3(t) (~7.9 wt%) and markedly higher sulfur (reported as SO_3 or total S) (~1.10 wt% vs ~0.15 wt% for the oxidized facies). Loss on ignition (LOI) is also higher in the sulfidic tailings (~9.59 wt% vs ~7.90 wt%),

consistent with greater volatile-bearing phases and/or residual carbonates/sulfides. Minor oxides remain low and comparable between facies (Na_2O ~1.7 - 1.8 wt%, K_2O ~2.1 - 2.3 wt%, TiO_2 ~0.62 - 0.65 wt%, MnO ~0.11 wt%, P_2O_5 ~0.08 - 0.09 wt%). Overall, the higher Fe and S contents in the sulfidic tailings, combined with differences in CaO + MgO, support facies-dependent reactivity and help interpret the differences in alkali demand and curing sensitivity discussed in Sections 3.1 and 4.4.

3.4.5. SEM Observations

SEM backscattered electron images (Figure 10) show continuous gel phases bridging tailings grains and progressive occlusion of intergranular pores in optimised mixes. In less reactive mixes, discrete reaction rims around unreacted grains, more open pore networks and local microcracking at grain-gel interfaces were observed. XRD patterns confirm quartz and feldspar dominance with accessory carbonates and sulfides in the raw tailings, and the appearance of broadened features associated with amorphous gels and minor secondary crystalline phases in cured products, consistent with alkali activation of a quartz-feldspar-carbonate framework under carbonate-buffered conditions.

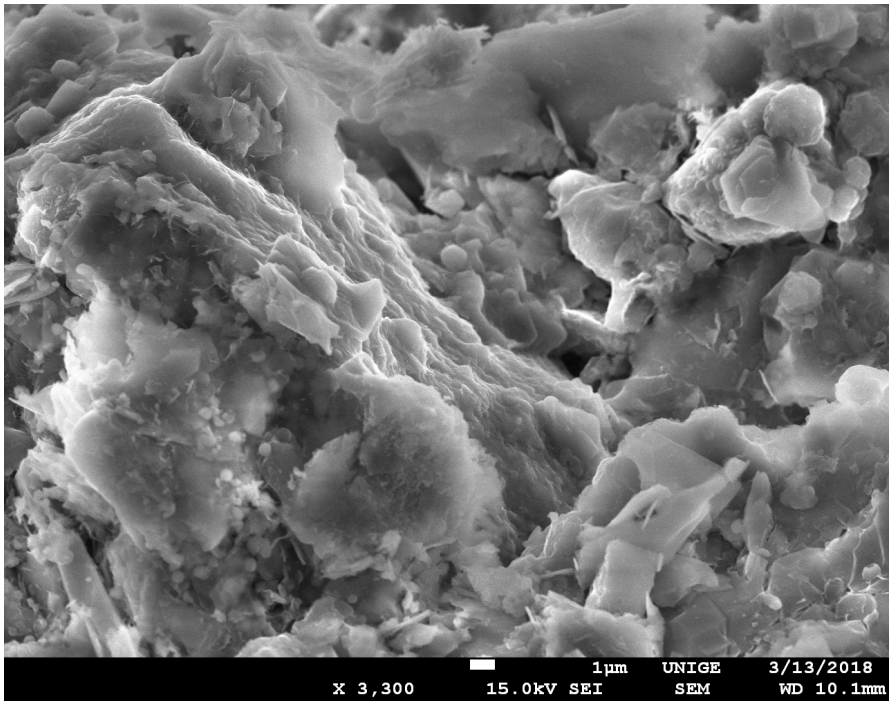

Figure 10. Representative SEM backscattered electron image of an optimised NaOH-activated Sabodala tailings mix, showing a dense reaction gel bridging angular tailings grains and partially occluding intergranular pores (scale bar = 1 µm).

FTIR spectra provide complementary evidence of the formation of aluminosilicate and carbonate-bearing reaction products, with shifts and broadening of Si-O-T bands and modifications in carbonate bands between raw tailings and cured mixes.

3.5. Product-Level Leaching

Product-level leaching tests on mechanically tested, crushed specimens showed low concentrations of potentially toxic elements in EN 12457-2 leachates across representative mixes spanning the selected formulation window. Table 5 presents, for As, Cd, Cr, Cu, Ni, Pb and Zn, the mean, minimum and maximum concentrations measured for selected mixes, together with indicative limit values compiled from European guidance documents on leaching from construction products and recycled materials, including Council Decision 2003/33/EC as transposed into waste acceptance criteria for inert and non-hazardous wastes.

Final leachate pH values are also reported in Table 5 to support interpretation of amphoteric metal behaviour in alkali-activated materials.

Table 5. EN 12457-2 leachate concentrations ($mg \cdot kg^{-1}$, dry mass basis) and final leachate pH for selected mixes, compared with indicative inert-waste limit values from Council Decision 2003/33/EC.

Element	Unit	Sabodala products - mean ($mg \cdot kg^{-1}$)	Min-max ($mg \cdot kg^{-1}$)	Indicative inert-waste limit ($mg \cdot kg^{-1}$)	Comment
As	$mg \cdot kg^{-1}$	0.02	0.01 - 0.03	0.5	~ one order of magnitude below limit
Cd	$mg \cdot kg^{-1}$	0.003	<0.002 - 0.005	0.04	Frequently below LOD; very low values
Cr	$mg \cdot kg^{-1}$	0.05	0.03 - 0.07	0.5	Well below limit
Cu	$mg \cdot kg^{-1}$	0.08	0.05 - 0.10	2	Well below limit
Ni	$mg \cdot kg^{-1}$	0.04	0.02 - 0.06	0.4	~ one order of magnitude below limit
Pb	$mg \cdot kg^{-1}$	0.03	0.02 - 0.05	0.5	Well below limit
Zn	$mg \cdot kg^{-1}$	0.3	0.20 - 0.40	4	One order of magnitude below limit
pH (final)		10.4	9.8 - 10.9		Measured after filtration

For context, the inert-waste limit values in Council Decision 2003/33/EC (applied at L/S = 10 $L \cdot kg^{-1}$ in EN 12457-type tests [33]) are of the order of 0.5 $mg \cdot kg^{-1}$ for As, 0.5 $mg \cdot kg^{-1}$ for Pb and 4 $mg \cdot kg^{-1}$ for Zn. In the present study, all mixes tested remained well below these values, typically by one to two orders of magnitude for the most critical elements (Table 5). Differences in leachate composition between cement and lime-bearing mixes were not statistically significant at $\alpha = 0.05$.

These comparisons are used solely as non-regulatory benchmarks: tests were conducted on laboratory-scale prisms, and any formal regulatory assessment would require testing on full-size units under the regulatory framework of the country of use. The data nevertheless indicate that alkali activation and the use of auxiliary binders do not measurably increase trace metal leachability relative to the as-deposited tailings. Within a proportionate, risk-based perspective, the leaching behavior appears compatible with reuse in non-load-bearing masonry units under controlled exposure conditions.

3.6. Durability Screening under Accelerated Protocols

Accelerated wet-dry cycling and sulfate exposure tests were performed on selected

mixes to provide a preliminary screening of durability. These tests were designed as screening-level indicators rather than full durability qualification, and were deliberately limited to a small number of specimens per condition (n = 3 - 4) and short exposure durations. For wet-dry cycling, representative specimens were subjected to up to 25 cycles of 24 h water immersion followed by 24 h oven drying at (50 ± 2)˚C. Mass changes over the cycles remained limited (mean values and standard deviations are reported in Table 6), and no significant scaling or major cracking was observed for mixes within the recommended formulation window. Flexural and compressive strengths measured after 10 and 25 cycles remained of the same order of magnitude as those of unexposed reference specimens, with changes generally within the scatter of replicate measurements (Table 6).

Table 6. Durability screening results for selected mixes under accelerated wet-dry cycling and sulfate exposure: mass change and strength retention.

Exposure condition	Mix ID	Facies	n	Mass change after 25 wet-dry cycles (%) (mean ± SD)	fc retention after 25 cycles (% of reference, mean)	ft retention after 25 cycles (% of reference, mean)	Mass change after 28 d sulfate exposure (%)	fc retention after sulfate exposure (% of reference, mean)
Wet-dry cycling	O-C3	Oxidized	3	+0.8 ± 0.6	88	84	-	-
Wet-dry cycling	S-C3	Sulfidic	3	+0.5 ± 0.5	90	86	-	-
Wet-dry cycling	O-L3	Oxidized	3	+1.2 ± 0.7	82	80	-	-
Wet-dry cycling	S-L3	Sulfidic	3	+0.9 ± 0.6	85	82	-	-
Sulfate (Na_2SO_4, 50 g·L^{-1}, 28 d)	O-C3	Oxidized	3	+1.0 ± 0.7	-	-	+1.0 ± 0.7	88
Sulfate ($MgSO_4$, 50 g·L^{-1}, 28 d)	S-C3	Sulfidic	3	+1.3 ± 0.8	-	-	+1.3 ± 0.8	85

Immersion in Na_2SO_4 and $MgSO_4$ solutions (50 g·L^{-1}) for 28 days led to modest mass variations and shallow reaction fronts, without severe cracking or spalling in optimised mixes. Phenolphthalein staining revealed limited alteration depths, and post-exposure strengths showed moderate decreases relative to reference values, typically on the order of 10% - 15%, again within the variability observed between specimens.

Given the limited number of specimens per condition (n = 3 - 4), the relatively short duration of the wet-dry (25 cycles) and sulfate (28 days) tests, and the fact that other degradation mechanisms such as carbonation, freeze-thaw cycling or combined mechanical and environmental loading were not investigated, these results cannot be used for any formal classification under particular masonry standards [23]-[26].

4. Discussion

4.1. Key Findings in the Context of Alkali-Activated Tailings

The results confirm that carbonate-buffered gold tailings from Sabodala can be

transformed into alkali-activated products with compressive strengths in the range typically reported for non-load-bearing masonry units, provided that mix design and curing are carefully controlled. Within the process window defined in Section 3.1, compressive strengths, water absorption and leaching behavior are broadly consistent with values reported for alkali-activated copper, iron or polymetallic tailings used in masonry-like products [1]-[3] [6] [12] [13] [15] [17]-[22]. In contrast to many of those previous studies, which focused on acid-generating tailings or paste-like binders [27]-[30], the present work explicitly addresses facies-specific mix design, flexural behavior and product-level leaching in a carbonate-buffered, near-neutral gold tailings system. The comparisons with EN 771-3 and ASTM C55 strength and absorption classes presented in Section 3.1 should therefore be interpreted as indicative benchmarks rather than evidence of formal conformity, since they are based on tests on 40 × 40 × 160 mm prisms rather than full-size masonry units.

The experimental campaign shows that NaOH molarity, activator solution fraction and auxiliary binder content can be combined to define a relatively narrow yet robust formulation window in which mechanical performance and leaching indicators are compatible with non-load-bearing masonry applications. The observation that total porosity varies only moderately between mixes, whereas strength and water absorption strongly depend on pore-size distribution, reinforces the interpretation that microstructural refinement (pore refinement, gel continuity) rather than bulk densification is the main driver of performance in these materials [37]. To the authors' knowledge, few previous studies on gold-mine tailings have simultaneously defined facies-specific alkali-activation windows and empirical ft-fc scaling laws for carbonate-buffered systems in a West African context, while jointly assessing mechanical, hydric and leaching performance at the product scale.

4.2. Facies-Specific Mix Design and Strength Scaling

Treating oxidized and sulfidic tailings as separate precursors proved essential for reliable mix design. The optimal activator solution fraction differs between facies (Section 3.1), reflecting their distinct particle size distributions, carbonate contents and reactivity. From a practical standpoint, this implies that facies should not be blended indiscriminately if consistent product performance is required. Instead, facies-specific envelopes of NaOH concentration and solution fraction can be defined and then adjusted for the available auxiliary binder and curing conditions.

The approximate proportionality between flexural-tensile and compressive strengths (Section 3.2) is also of practical importance. Although the ft-fc relationships obtained here are empirical and limited to the tested fc range (~8 - 22 MPa), they provide a rational basis for estimating flexural performance from compressive tests. Outside this fc range, the ft-fc relationships should be used with caution and, where possible, supported by additional testing. This is attractive for small

laboratories or production facilities where routine flexural testing may not be feasible. In a screening or quality-control context, compressive strength can thus be used as the primary control parameter, with simple ft-fc relations providing indicative flexural ranges and safety factors [38]-[40].

4.3. Environmental Performance and Leaching

At the product scale, EN 12457-2 leachates [33] from crushed, cured specimens remained low for all mixes tested (Section 3.5). In several cases, leachate concentrations for selected elements were close to or below detection limits, and when compared with indicative limit values compiled from European guidance documents for construction products and recycled materials, they fall well within those bounds (**Table 5**). Although this comparison is not a formal regulatory assessment, it suggests that alkali activation and the use of auxiliary binders do not aggravate trace metal mobility relative to the as-deposited tailings. These comparisons with inert waste acceptance criteria (e.g., European Council Decision 2003/33/EC) are therefore used only as indicative, non-regulatory benchmarks; any formal compliance assessment would require testing full-size units under the relevant national regulatory framework.

The combination of carbonate buffering in the tailings and the formation of dense, continuous reaction products likely contributes to this behavior by limiting pH excursions and reducing pore connectivity at the scale relevant for leaching. From a risk-based perspective, such performance is encouraging: it indicates that, if units are used in appropriate exposure conditions and under suitable regulatory oversight, environmental risks need not be a primary barrier to reuse. Nonetheless, longer-term leaching tests, and tests on full-size units under more realistic exposure scenarios, remain necessary before any final conclusions can be drawn.

4.4. Practical Implementation, Energy and Socio-Economic Considerations

From a practical standpoint, the requirement for elevated-temperature curing is one of the most critical aspects of the proposed process. The 210˚C, 4 h schedule used here should therefore be viewed as an upperbound, screening regime, chosen to delineate a robust activation window and to enable meaningful comparison between mix designs. Although this regime is far milder than typical clay-brick firing, it remains more energy-intensive than ambient or low-temperature curing of Portland cement masonry units, and future work should focus on lowering curing temperature and/or time while maintaining acceptable strength and absorption.

In a West African context, where electricity and fuel costs can be high and supply reliability variable, implementing a 210˚C/4 h cure at scale would therefore require careful consideration. Several mitigation strategies can be envisaged: using waste heat from on-site power plants; integrating solar thermal assistance where feasible; reducing curing time once minimum strength is reached; or lowering the target temperature for mixes that show sufficient reactivity. Importantly, reaching

~210˚C is generally beyond conventional flat-plate collectors and many standard solar-thermal systems; it would more realistically rely on concentrating solar thermal technologies (e.g., parabolic trough or linear Fresnel) or high-temperature evacuated-tube configurations with concentrators, which has implications for the techno-economic feasibility [41]. An industrial process would likely operate within a narrower, optimised curing window than the one explored experimentally here, balancing strength, energy consumption and throughput.

The socio-economic attractiveness of such a process must be evaluated against realistic alternatives. One baseline scenario is continued surface storage of tailings in the TSF, with associated long-term monitoring and rehabilitation costs, combined with production or importation of conventional masonry units (clay bricks, concrete blocks). In contrast, converting a fraction of the TSF into masonry units would: (i) reduce the volume of tailings requiring long-term management, (ii) create a local source of construction materials, and (iii) potentially generate employment and business opportunities for small and medium-sized enterprises near the mine.

The total volume of tailings in a large TSF is such that even a relatively small fraction being upgraded into masonry units could correspond to many years of local brick or block production. In practice, the fraction that can be realistically valorised will be limited by logistical constraints (distance to markets, handling and processing capacity), by market demand for non-load-bearing units, and by the willingness of mine operators, local authorities and SMEs to codevelop such schemes. Integrated models could emerge in which the mine provides access to tailings, technical support and possibly curing infrastructure, while local SMEs handle moulding, curing and distribution, under a regulatory framework that ensures environmental and safety standards.

Ultimately, the feasibility of implementing NaOH-activated tailings-based masonry units in Senegal or elsewhere in West Africa will depend not only on technical performance but also on the relative costs of activators and energy, the availability of alternative materials, institutional support for circular economy approaches and the existence of standards or guidelines that recognise such products. The present work provides technical evidence that mechanically and environmentally acceptable products are achievable; it does not by itself resolve the economic and institutional dimensions, which require dedicated analysis [42] [43].

4.5. Limitations and Future Research Needs

Several limitations of the present study must be acknowledged. First, all results are based on laboratory-scale prisms produced under controlled conditions; full-size blocks or units may exhibit different behavior due to scale effects, compaction methods, drying gradients and handling. Second, the curing regime explored here is relatively high in temperature and short in duration. While this was necessary to obtain robust trends and clearly identify a formulation window, it leaves open

the question of how far curing temperatures and times can be reduced while maintaining acceptable performance.

Third, the durability assessment was limited to short-term wet-dry cycling and sulfate exposure under accelerated but simplified laboratory conditions (Section 3.6). Other degradation mechanisms such as carbonation, freeze-thaw (for colder climates), chloride ingress or combined mechanical and environmental loading were not studied. Long-term field exposure trials and extended laboratory test campaigns on full-size units would be required before any formal durability class could be assigned.

Finally, although the methodological framework developed here—facies-based characterisation, structured mix-design exploration, and joint evaluation of strength, water absorption, leaching and preliminary durability—is intended to be transferable, its application to other sites will require adaptation. Tailings with different mineralogies (e.g., more acid-generating, less carbonate-buffered, or with higher clay contents) may respond differently to NaOH activation and may require different activators, binder blends or curing regimes.

Future work should therefore focus on: 1) validating the proposed process window on full-size units produced with realistic forming and curing technologies, 2) exploring lower-energy curing schedules and alternative activators or hybrid binders, 3) conducting extended durability and leaching tests under more realistic exposure conditions, and 4) embedding the technical findings into techno-economic and life-cycle assessments that can guide decision-makers on the relative merits of tailings-based masonry units versus conventional construction products.

5. Conclusions

This study investigated the potential of NaOH-activated tailings from the Sabodala gold mine (Senegal) as precursors for non-load-bearing masonry units, with a focus on facies-specific mix design, mechanical strength, water absorption and product-level leaching. Within the range of conditions explored, the results strongly suggest that both oxidized and sulfidic tailings can be converted into alkali-activated products with compressive strengths and absorption characteristics broadly compatible with non-load-bearing masonry classes, provided that activator content, auxiliary binder dosage and curing regime are carefully controlled.

The experimental programme showed that NaOH molarity and activator solution fraction are first-order drivers of strength, with facies-dependent optimum solution fractions around 21 wt% for oxidized tailings and 18 wt% for sulfidic tailings. Small additions of Portland cement or hydrated lime (~3 wt%) further improved strength and, in cement-bearing mixes, reduced water absorption. Within this facies-specific process window and using a reference curing schedule of 210˚C for 4 h, representative 28-day compressive strengths in the 12 - 20 MPa range and 24 h water absorption values around 10% - 15% were obtained. Within this window, dry density values for cured prisms typically ranged around 17 - 19

$kN \cdot m^{-3}$, consistent with medium-density non-load-bearing masonry units. Flexural-tensile strength scaled approximately linearly with compressive strength (ft ~ 0.26 - 0.27 fc for 8 - 22 MPa), providing practical scaling laws that could support compressive-only quality control in a screening or production context.

Product-level EN 12457-2 leaching tests on crushed, cured specimens yielded low concentrations of As, Pb, Zn and other elements of concern, which remained within indicative limit values compiled from European guidance documents for construction products and recycled materials. Although these comparisons are non-regulatory and based on laboratory-scale prisms, they indicate that alkali activation and auxiliary binders do not measurably increase trace metal leachability relative to the as-deposited tailings. Short-term durability screening under wet-dry cycling and sulfate exposure suggested a basic level of resistance consistent with non-structural masonry applications under controlled exposure conditions, but further work is required to confirm long-term performance and compliance with specific durability standards.

Several important limitations must be kept in mind. All mechanical, leaching and durability results were obtained on small prisms under controlled laboratory conditions, using a relatively high curing temperature and a limited set of exposure scenarios. The conclusions therefore apply within the tested conditions and parameter ranges, and cannot be directly extrapolated to full-size industrial units or to markedly different curing regimes. Future work should address full-scale production trials, lower-energy curing schedules, extended durability testing and techno-economic assessments before any formal qualification of these materials under masonry standards can be attempted. The durability results reported here should therefore be interpreted strictly as short-term screening outcomes.

Beyond the specific case of Sabodala, the approach used in this study provides a screening framework that can be adapted to other tailings storage facilities, particularly in West Africa and similar settings. In practical terms, such a framework involves at least three main steps:

- Facies-based characterisation, combining geotechnical, mineralogical and geochemical data to identify candidate tailings facies and assess their environmental baseline (e.g., acid-generating vs carbonate-buffered behavior);
- Structured mix-design exploration within a realistic window of activator, auxiliary binder and curing conditions, supported by simple statistical tools to identify robust, facies-specific formulation windows;
- Combined evaluation of performance, including compressive and flexural strength, water absorption, product-level leaching and preliminary durability, benchmarked against relevant non-load-bearing masonry requirements and indicative environmental limits.

Applied in a proportionate and site-specific way, this framework can help mine operators, regulators and local stakeholders to identify situations where turning geochemically benign tailings into masonry units is technically promising, and where more detailed scale-up and economic studies are warranted.

Acknowledgements

We thank Sabodala Gold Operations for sampling permissions and logistics, and for analytical support.

Conflicts of Interest

The authors declare no conflicts of interest regarding the publication of this paper.

References

[1] Kiventerä, J., Perumal, P., Yliniemi, J. and Illikainen, M. (2020) Mine Tailings as a Raw Material in Alkali Activation: A Review. *International Journal of Minerals, Metallurgy and Materials*, **27**, 1009-1020. https://doi.org/10.1007/s12613-020-2129-6

[2] Mabroum, S., Moukannaa, S., El Machi, A., Taha, Y., Benzaazoua, M. and Hakkou, R. (2020) Mine Wastes Based Geopolymers: A Critical Review. *Cleaner Engineering and Technology*, **1**, Article ID: 100014. https://doi.org/10.1016/j.clet.2020.100014

[3] Manaviparast, H.R., Miranda, T., Pereira, E. and Cristelo, N. (2024) A Comprehensive Review on Mine Tailings as a Raw Material in the Alkali Activation Process. *Applied Sciences*, **14**, Article No. 5127. https://doi.org/10.3390/app14125127

[4] Guo, Y., Qu, F. and Li, W. (2025) Advancing Circular Economy and Construction Sustainability: Transforming Mine Tailings into High-Value Cementitious and Alkali-Activated Concrete. *NPJ Materials Sustainability*, **3**, Article No. 8. https://doi.org/10.1038/s44296-025-00049-9

[5] Palomo, A., Grutzeck, M.W. and Blanco, M.T. (1999) Alkali-Activated Fly Ashes: A Cement for the Future. *Cement and Concrete Research*, **29**, 1323-1329. https://doi.org/10.1016/s0008-8846(98)00243-9

[6] Davidovits, J. (2008) Geopolymer Chemistry and Applications. Geopolymer Institute.

[7] Provis, J.L. and van Deventer, J.S.J., Eds. (2014) Alkali Activated Materials: State-of-the-Art Report, RILEM TC 224-AAM. Springer.

[8] Luukkonen, T., Abdollahnejad, Z., Yliniemi, J., Kinnunen, P. and Illikainen, M. (2018) One-Part Alkali-Activated Materials: A Review. *Cement and Concrete Research*, **103**, 21-34. https://doi.org/10.1016/j.cemconres.2017.10.001

[9] Provis, J.L. (2018) Alkali-Activated Materials. *Cement and Concrete Research*, **114**, 40-48. https://doi.org/10.1016/j.cemconres.2017.02.009

[10] Fernández-Jiménez, A. and Palomo, A. (2003) Characterisation of Fly Ashes. Potential Reactivity as Alkaline Cements. *Fuel*, **82**, 2259-2265. https://doi.org/10.1016/s0016-2361(03)00194-7

[11] Puertas, F. and Fernández-Jiménez, A. (2003) Mineralogical and Microstructural Characterisation of Alkali-Activated Fly Ash/Slag Pastes. *Cement and Concrete Composites*, **25**, 287-292. https://doi.org/10.1016/s0958-9465(02)00059-8

[12] Fang, G., Ho, W.K., Tu, W. and Zhang, M. (2018) Workability and Mechanical Properties of Alkali-Activated Fly Ash-Slag Concrete Cured at Ambient Temperature. *Construction and Building Materials*, **172**, 476-487. https://doi.org/10.1016/j.conbuildmat.2018.04.008

[13] Amer, I., Kohail, M., El-Feky, M.S., Rashad, A. and Khalaf, M.A. (2021) A Review on Alkali-Activated Slag Concrete. *Ain Shams Engineering Journal*, **12**, 1475-1499. https://doi.org/10.1016/j.asej.2020.12.003

[14] Krishna, R.S., Shaikh, F., Mishra, J., Lazorenko, G. and Kasprzhitskii, A. (2021) Mine Tailings-Based Geopolymers: Properties, Applications and Industrial Prospects. *Ceramics International*, **47**, 17826-17843. https://doi.org/10.1016/j.ceramint.2021.03.180

[15] Van Jaarsveld, J.G.S., Van Deventer, J.S.J. and Lorenzen, L. (1997) The Potential Use of Geopolymeric Materials to Immobilise Toxic Metals: Part I. Theory and Applications. *Minerals Engineering*, **10**, 659-669. https://doi.org/10.1016/s0892-6875(97)00046-0

[16] He, X. (2022) Mine Tailings-Based Geopolymers: Durability, Microstructure, Thermal and Leaching Properties.

[17] Caballero, E., Sánchez, W. and Ríos, C.A. (2014) Synthesis of Geopolymers from Alkaline Activation of Gold Mining Wastes. *Ingeniería y Competitividad*, **16**, 317-330. https://doi.org/10.25100/iyc.v16i1.3735

[18] Kiventerä, J., Lancellotti, I., Catauro, M., Poggetto, F.D., Leonelli, C. and Illikainen, M. (2018) Alkali Activation as New Option for Gold Mine Tailings Inertization. *Journal of Cleaner Production*, **187**, 76-84. https://doi.org/10.1016/j.jclepro.2018.03.182

[19] Yao, G., Liu, Q., Wang, J., Wu, P. and Lyu, X. (2019) Effect of Mechanical Grinding on Pozzolanic Activity and Hydration Properties of Siliceous Gold Ore Tailings. *Journal of Cleaner Production*, **217**, 12-21. https://doi.org/10.1016/j.jclepro.2019.01.175

[20] Morales Aranibar, C.G., La Rosa Toro Gómez, A., da Silva, J.L., Morales-Aranibar, L. and Arán, D. (2025) Reuse of Mine Tailings through Geopolymerization Applied to 3D Printing: A Review of Progress, Challenges and Perspectives. *Sustainability*, **17**, Article No. 2617. https://doi.org/10.3390/su17062617

[21] Ahmari, S. and Zhang, L. (2013) Durability and Leaching Behavior of Mine Tailings-Based Geopolymer Bricks. *Construction and Building Materials*, **44**, 743-750. https://doi.org/10.1016/j.conbuildmat.2013.03.075

[22] Thejas, H.K. and Hossiney, N. (2022) Alkali-Activated Bricks Made with Mining Waste Iron Ore Tailings. *Case Studies in Construction Materials*, **16**, e00973. https://doi.org/10.1016/j.cscm.2022.e00973

[23] CEN (2015) EN 771-1:2011+A1:2015 Specification for Masonry Units-Part 1: Clay Masonry Units. European Committee for Standardization.

[24] CEN (2015) EN 771-3:2011+A1:2015 Specification for Masonry Units-Part 3: Aggregate Concrete Masonry Units (Dense and Lightweight Aggregates). European Committee for Standardization.

[25] ASTM International (2021) ASTM C67/C67M-21 Standard Test Methods for Sampling and Testing Brick and Structural Clay Tile. ASTM International.

[26] ASTM International (2023) ASTM C62-23 Standard Specification for Building Brick (Solid Masonry Units Made from Clay or Shale). ASTM International.

[27] Nordstrom, D.K. and Alpers, C.N. (1997) Geochemistry of Acid Mine Waters. In: Plumlee, G.S. and Logsdon, M.J., Eds., *The Environmental Geochemistry of Mineral Deposits*, *Part A*: *Processes*, *Methods*, *and Health Issues*, Society of Economic Geologists, 133-160. https://doi.org/10.5382/rev.06.06

[28] Blowes, D.W., Ptacek, C.J., Jambor, J.L. and Weisener, C.G. (2003) The Geochemistry of Acid Mine Drainage. In: Jambor, J.L., Blowes, D.W. and Ritchie, A.I.M., Eds., *Environmental Aspects of Mine Wastes*, Mineralogical Association of Canada, 149-204. https://doi.org/10.1016/b0-08-043751-6/09137-4

[29] Lindsay, M.B.J., Moncur, M.C., Bain, J.G., Jambor, J.L., Ptacek, C.J. and Blowes, D.W. (2015) Geochemical and Mineralogical Aspects of Sulfide Mine Tailings. *Applied Ge-*

ochemistry, **57**, 157-177. https://doi.org/10.1016/j.apgeochem.2015.01.009

[30] Park, I., Tabelin, C.B., Jeon, S., Li, X., Seno, K., Ito, M., *et al.* (2019) A Review of Recent Strategies for Acid Mine Drainage Prevention and Mine Tailings Recycling. *Chemosphere*, **219**, 588-606. https://doi.org/10.1016/j.chemosphere.2018.11.053

[31] CEN (2011) EN 197-1:2011 Cement-Part 1: Composition, Specifications and Conformity Criteria for Common Cements. European Committee for Standardization.

[32] ASTM International (2018) ASTM C1012/C1012M-18b Standard Test Method for Length Change of Hydraulic-Cement Mortars Exposed to a Sulfate Solution. ASTM International.

[33] CEN (2002) EN 12457-2:2002 Characterisation of Waste-Leaching-Compliance Test for Leaching of Granular Waste Materials and Sludges-Part 2: One Stage Batch Test at a Liquid to Solid Ratio of 10 L/kg for Materials with Particle Size below 4 mm (without or with Size Reduction). European Committee for Standardization.

[34] Washburn, E.W. (1921) The Dynamics of Capillary Flow. *Physical Review*, **17**, 273-283. https://doi.org/10.1103/physrev.17.273

[35] Tibbetts, C.M., Tao, C., Paris, J.M. and Ferraro, C.C. (2020) Mercury Intrusion Porosimetry Parameters for Use in Concrete Penetrability Qualification Using the Katz-Thompson Relationship. *Construction and Building Materials*, **263**, Article ID: 119834. https://doi.org/10.1016/j.conbuildmat.2020.119834

[36] ASTM International (2025) ASTM C55-25: Standard Specification for Dry-Cast Concrete Building Brick. ASTM International.

[37] Lv, Y., Wang, C., Han, W., Li, X. and Peng, H. (2023) Study of the Mechanical Properties and Microstructure of Alkali-Activated Fly Ash-Slag Composite Cementitious Materials. *Polymers*, **15**, Article No. 1903. https://doi.org/10.3390/polym15081903

[38] Dhevaraju, L., Reddy, E.A., Dogiparthy, N.D. and Kar, A. (2019) Relationship between Flexural and Compressive Strength of Concrete Made of Alkali Activated Binder. In: Dasgupta, K., Ed., *National Conference on Structural Engineering and Construction Management*, Springer International Publishing, 139-145. https://doi.org/10.1007/978-3-030-26365-2_13

[39] Li, B., Wu, F., Xia, D., Li, Y., Cui, K., Wu, F., *et al.* (2023) Compressive and Flexural Behavior of Alkali-Activated Slag-Based Concrete: Effect of Recycled Aggregate Content. *Journal of Building Engineering*, **67**, Article ID: 105993. https://doi.org/10.1016/j.jobe.2023.105993

[40] Tajunnisa, Y., Rasuli, M.I., Yamamura, A. and Shigeishi, M. (2023) Reliability Prediction of Alkali-Activated Mortar during Flexural Loading Using Weibull Analysis. *Heliyon*, **9**, e21512. https://doi.org/10.1016/j.heliyon.2023.e21512

[41] IEA-ETSAP and IRENA (2015) Solar Heat for Industrial Processes: Technology Brief E21. International Renewable Energy Agency (IRENA).

[42] Pol Segura, I., Ranjbar, N., Juul Damø, A., Skaarup Jensen, L., Canut, M. and Arendt Jensen, P. (2023) A Review: Alkali-Activated Cement and Concrete Production Technologies Available in the Industry. *Heliyon*, **9**, e15718. https://doi.org/10.1016/j.heliyon.2023.e15718

[43] Ricciotti, L., Lucariello, D., Perrotta, V., Apicella, A. and Aversa, R. (2025) Sustainable Alkali-Activated and Geopolymer Materials: What Is the Future for Italy? *Recycling*, **10**, Article No. 140. https://doi.org/10.3390/recycling10040140